Fast and Unconditional All-Microwave Reset of a Superconducting Qubit

P. Magnard, P. Kurpiers, B. Royer, T. Walter, J.-C. Besse, S. Gasparinetti, M. Pechal, J. Heinsoo, S. Storz, A. Blais, and A. Wallraff

Phys. Rev. Lett. **121**, 060502 — Published 7 August 2018

DOI: 10.1103/PhysRevLett.121.060502

Fast and Unconditional All-Microwave Reset of a Superconducting Qubit

P. Magnard,[1] P. Kurpiers,[1] B. Royer,[2] T. Walter,[1] J.-C. Besse,[1] S. Gasparinetti,[1]
M. Pechal,[1] J. Heinsoo,[1] S. Storz,[1] A. Blais,[2,3] and A. Wallraff[1]

[1] *Department of Physics, ETH Zürich, CH-8093 Zürich, Switzerland.*
[2] *Institut Quantique and Département de Physique, Université de Sherbrooke, Sherbrooke, Québec J1K 2R1, Canada*
[3] *Canadian Institute for Advanced Research, Toronto, ON, Canada*

(Dated: June 22, 2018)

Active qubit reset is a key operation in many quantum algorithms, and particularly in quantum error correction. Here, we experimentally demonstrate a reset scheme for a three-level transmon artificial atom coupled to a large bandwidth resonator. The reset protocol uses a microwave-induced interaction between the $|f,0\rangle$ and $|g,1\rangle$ states of the coupled transmon-resonator system, with $|g\rangle$ and $|f\rangle$ denoting the ground and second excited states of the transmon, and $|0\rangle$ and $|1\rangle$ the photon Fock states of the resonator. We characterize the reset process and demonstrate reinitialization of the transmon-resonator system to its ground state in less than 500 ns and with 0.2% residual excitation. Our protocol is of practical interest as it has no additional architectural requirements, beyond those needed for fast and efficient single-shot readout of transmons, and does not require feedback.

The efficient initialization of a set of qubits into their ground state is one of the DiVincenzo criteria for quantum information processing [1]. Initialization is also critical for the implementation of error correction codes [2–4] to reset ancilla qubits on demand to a fiducial state in short time and with high fidelity. For this reason, qubit reset procedures have been implemented for a wide range of physical quantum computation platforms [5–9], including superconducting qubits for which we discuss the most common approaches below [10–19].

Reset for superconducting qubits is commonly realized using the outcome of a strong projective measurement to either herald the ground state [13] or deterministically prepare it using feedback [14–17]. Measurement-induced state mixing limits the achievable single-shot readout fidelity and the performance of this approach [16, 20, 21]. In addition, measurement-induced mixing constrains the quantum-non-demolition nature of dispersive readout giving rise to leakage out of the qubit subspace [16, 22], which is particularly detrimental to quantum error correction [23].

Alternatively, qubit reset can be achieved by coupling the qubit excited state to a cold and rapidly decaying quantum system. Such driven reset schemes [10, 11, 18, 24, 25] make use of ideas related to dissipation engineering [26–29]. In one variant of this approach [11], the qubit is quickly tuned into resonance with a Purcell filtered, large-bandwidth, resonator using magnetic flux. The qubit then quickly thermalizes to its ground state due to Purcell decay, the rate of which can be adjusted, on-demand, by three orders of magnitude. The flux pulses employed in this scheme require careful calibration, they may affect subsequent gates by bleedthrough and neighboring qubits through cross-talk [30].

An all-microwave reset protocol utilizing the qubit-state-dependent response of a resonator [18] avoids the use of flux tuning and its potentially detrimental effects. This protocol [18] has minimal hardware requirements, only a single resonator, but requires a cavity linewidth κ smaller than the dispersive interaction strength χ limiting both the speed of the reset process and the readout if the same resonator is used [31, 32].

In this work, we demonstrate an alternative all-microwave reset protocol of a three-level transmon coupled to a resonator with no constraint on κ. Driving the transmon simultaneously with two coherent tones forms a Λ system in the Jaynes-Cumming ladder [33] and unconditionally transfers any excitation in the two lowest excited states of the transmon to a single-photon emitted to the environment, thus resetting the transmon qutrit on-demand. This protocol outperforms existing measurement-based and all-microwave driven reset schemes in speed and fidelity [34], populates the resonator with one photon at most, and can be extended to other types of superconducting qubits. In addition, this protocol is of practical interest as it is optimized when the resonator is designed for rapid and high-fidelity transmon readout [32].

The device used in our experiment and schematically illustrated in Fig. 1a, uses a transmon qubit [35, 36] (orange), with transition frequency $\omega_{\mathrm{ge}}/2\pi = 6.343\,\mathrm{GHz}$, anharmonicity $\alpha/2\pi = -265\,\mathrm{MHz}$ and energy relaxation time $T_1 = 5.5\,\mu\mathrm{s}$. We control the qubit state with microwave pulses up-converted from an arbitrary waveform generator (AWG), applied to the transmon through a dedicated drive line. To perform the reset, the transmon is capacitively coupled with rate $g_{\mathrm{r}}/2\pi = 335\,\mathrm{MHz}$ to a resonator of frequency $\omega_{\mathrm{r}}/2\pi = 8.400\,\mathrm{GHz}$, resulting in a dispersive interaction with rate $\chi_{\mathrm{r}}/2\pi = -6.3\,\mathrm{MHz}$ (light blue). The reset resonator is connected through a Purcell-filter resonator to cold $50\,\Omega$ loads with an effective coupling $\kappa/2\pi = 9\,\mathrm{MHz}$. This resonator can, in

principle, be used for transmon readout. However, in the present work, to decouple the reset from its characterization process, we read out the transmon with a dedicated, Purcell-filtered resonator (light green). We present further details about the sample in the Supplemental Material [34].

We read out the transmon state using a gated drive applied to the input port of the readout resonator at a frequency optimized for qutrit readout [37]. The signal scattered off the readout resonator is amplified at $T_{\mathrm{BT}} = 10\,\mathrm{mK}$ by a Josephson parametric amplifier [38, 39]. The signal is then amplified at 4 K with high electron mobility transistors, down-converted using an I-Q mixer, digitized using an analog-to-digital converter, digitally down-converted and processed using a field programmable gate array.

The reset concept, illustrated in Fig. 1b, is based on a cavity-assisted Raman transition between $|f,0\rangle$ and $|g,1\rangle$ [33, 40, 41]. Here, $|s,n\rangle$ denotes the tensor product of the transmon in state $|s\rangle$, with its three lowest energy eigenstates $|g\rangle$, $|e\rangle$ and $|f\rangle$, and the reset resonator in the n photon Fock state $|n\rangle$. By simultaneously driving the $|f,0\rangle \leftrightarrow |g,1\rangle$ (f0-g1) transition and the $|e,0\rangle \leftrightarrow |f,0\rangle$ (e-f) transition, the population is transferred from the qutrit excited states, $|e,0\rangle$ and $|f,0\rangle$, to the state $|g,1\rangle$. The system then rapidly decays to the target dark state $|g,0\rangle$ by photon emission at rate κ, effectively resetting the qutrit to its ground state.

We model the dynamics of the reset by the non-Hermitian Hamiltonian

$$H/\hbar = \begin{bmatrix} -\delta_{\mathrm{ef}} & \Omega_{\mathrm{ef}} & 0 \\ \Omega_{\mathrm{ef}}^{*} & 0 & \tilde{g} \\ 0 & \tilde{g}^{*} & -\delta_{\mathrm{f0g1}} - i\kappa/2 \end{bmatrix}, \qquad (1)$$

acting on the states $|e,0\rangle$, $|f,0\rangle$ and $|g,1\rangle$. Here, the non-Hermitian term $-i\kappa/2$ accounts for the photon emission process, and Ω_{ef} and $\tilde{g}$ are the e-f and f0-g1 drive-induced Rabi rates, respectively. Because the f0-g1 drive acts on a second order-transition, it requires a high amplitude V_{f0g1} and induces significant ac Stark shifts $\bar{\Delta}_{\mathrm{ef}}$ and $\bar{\Delta}_{\mathrm{f0g1}}$ of the e-f and f0-g1 transitions [40]. In Hamiltonian (1), δ_{ef} and δ_{f0g1} denote the detuning of the drives from their respective ac Stark shifted transitions. Therefore, gaining experimental control over the reset drive parameters requires to characterize the dependence of $\bar{\Delta}_{\mathrm{ef}}$ and $\bar{\Delta}_{\mathrm{f0g1}}$ on V_{f0g1} as well as the relation between the drive amplitudes and their corresponding Rabi rates.

First, we determine the ac Stark shift $\bar{\Delta}_{\mathrm{f0g1}}$. We initialize the transmon in $|g\rangle$, then apply a sequence of two π-pulses (π_{ge}, π_{ef}) to prepare the system in $|f,0\rangle$ (Fig. 1c). We apply a flat top f0-g1 pulse of carrier frequency ν_{f0g1}, amplitude V_{f0g1} and duration t_{r} and read out the resulting transmon state populations. Here and in all calibration measurements, the populations $P_{\mathrm{g,e,f}}$ of the transmon qutrit are extracted by comparing the averaged signal transmitted through the readout resonator to

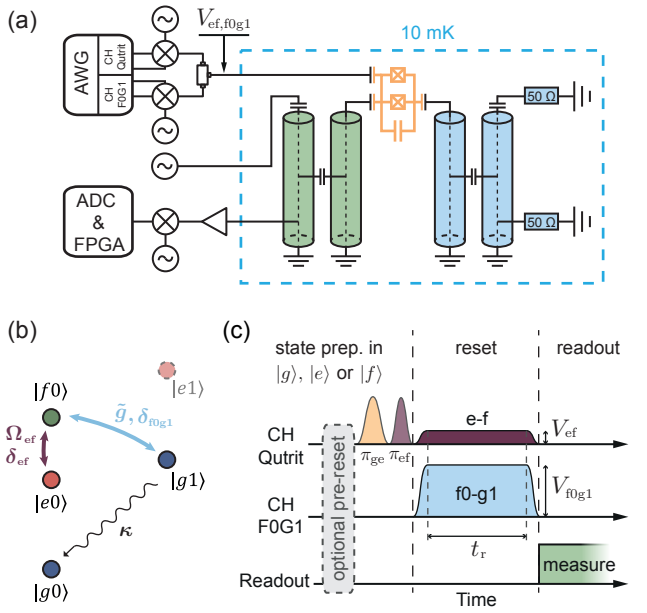

FIG. 1. (a) Simplified schematic of the experimental setup. A transmon (orange) is coupled to two Purcell-filtered resonators. The readout resonator (green) is connected to room temperature electronics (description in the main text), while the reset resonator (blue) is connected to two 50 Ω loads thermalized at base temperature. (b) Jaynes-Cummings ladder diagram of the transmon/reset resonator energy levels. The purple and light blue arrows represent the e-f and f0-g1 pulsed coherent drives, respectively, and the black arrow labelled κ illustrates the resonator decay process. (c) Illustration of the pulse schemes used to test the reset protocol. We initialize the qutrit to its ground state passively or optionally with an unconditional reset, then prepare the desired state $|g\rangle$, $|e\rangle$ or $|f\rangle$ with control pulses (labelled π_{ge} and π_{ef}). We reset the qutrit by simultaneously applying flat-top e-f (purple) and f0-g1 (light blue) pulses for a reset time t_{r}. The resulting qutrit state is then measured by applying a microwave tone to the readout resonator (green).

reference traces [37]. We repeat the process varying ν_{f0g1} and V_{f0g1}, while keeping $V_{\mathrm{f0g1}}t_{\mathrm{r}}$ fixed to obtain comparable Rabi angles for the rotations induced by the f0-g1 drive. For a given value of V_{f0g1}, we fit the dependence of P_{g} on ν_{f0g1} to a Gaussian whose center yields the ac Stark shifted frequency, at which the population transfer from $|f,0\rangle$ to $|g,1\rangle$ is maximized (Fig. 2a). The ac Stark shift $\bar{\Delta}_{\mathrm{f0g1}}$ extracted in this way shows a quadratic dependence on V_{f0g1} (blue diamonds in Fig. 2b).

To determine $\bar{\Delta}_{\mathrm{ef}}$, we prepare the system in $|e,0\rangle$ and apply a short square e-f π-pulse of frequency ν_{ef} in the presence of a continuous, resonant f0-g1 drive of amplitude V_{f0g1}. For each V_{f0g1}, we extract the ac Stark shifted frequency of the e-f transition by finding the minimum of P_{e} *vs.* ν_{ef} with a fit to a Gaussian (Fig. 2c). As before, we observe a quadratic dependence of $\bar{\Delta}_{\mathrm{ef}}$ on V_{f0g1} (purple triangles in Fig. 2b).

Finally, we perform resonant Rabi oscillation measure-

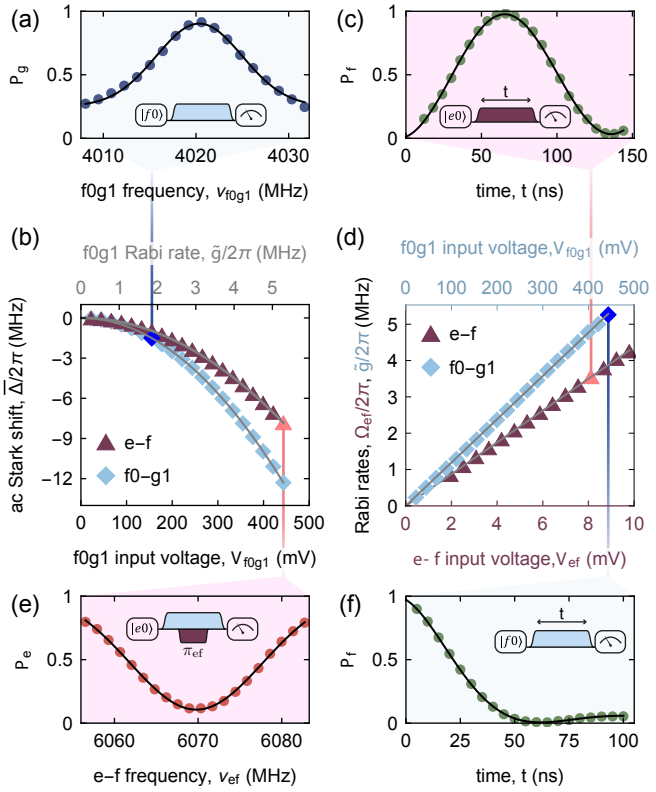

FIG. 2. (a) Population P_g *vs.* the frequency ν_{f0g1} of a flat-top f0-g1 pulse, of amplitude V_{f0g1}, applied to the qutrit initially prepared in $|f,0\rangle$. (b) Measured ac Stark shifts $\bar{\Delta}_{f0g1}$ and $\bar{\Delta}_{ef}$ of the f0-g1 (blue diamonds) and e-f (purple triangles) transitions, *vs.* amplitude V_{f0g1} of the f0-g1 drive. The solid lines are quadratic fits to the data. (c) Population P_e *vs.* frequency ν_{ef} of a flat-top e-f π-pulse applied on the qutrit, initially prepared in state $|e,0\rangle$, in the presence of a continuous f0-g1 drive of amplitude V_{f0g1}. (d) Population P_f *vs.* duration t of a resonant flat-top e-f pulse, of amplitude $V_{ef} = 8\,\text{mV}$. (e) Extracted Rabi rates Ω_{ef} and $\tilde{g}$, of the e-f (purple trianlges) and f0-g1 (blue diamonds) drives versus their amplitude, V_{ef} and V_{f0g1}. The solid lines are linear fits. (f) Population P_f *vs.* duration t of a resonant square f0-g1 pulse, of amplitude $V_{f0g1} = 444\,\text{mV}$. The pulse schemes used to acquire the data shown in panels (a), (c), (d) and (f) are shown as insets, with the f0-g1 and e-f pulse envelopes represented in blue and purple, respectively. The solid lines in (a) and (c) are fits to Gaussians. The solid lines in (c) and (f) are fits to Rabi oscillation models described in Ref. [34].

ments on the e-f and f0-g1 transitions to extract the linear relation between the drive amplitudes V_{ef} and V_{f0g1}, and their corresponding Rabi rates [34] (Fig. 2d, e, f). The Rabi oscillations between $|f,0\rangle$ and $|g,1\rangle$ are damped due to the spontaneous decay from $|g,1\rangle$ to $|g,0\rangle$ (Fig. 2f).

In all following experiments, we adjust the drive frequencies such that $\delta_{ef} = \delta_{f0g1} = 0$ to reset the transmon, leaving only $\tilde{g}$ and Ω_{ef} as tunable parameters. From

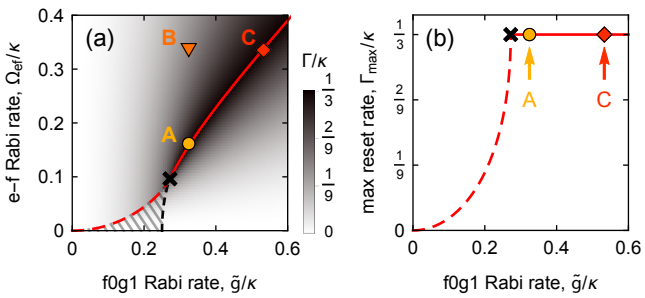

FIG. 3. (a) Calculated reset rate Γ/κ, *vs.* Rabi rates $\tilde{g}/\kappa$ and Ω_{ef}/κ. The over-damped parameter region is hatched. The red line shows the values of Ω_{ef} maximizing Γ as a function of $\tilde{g}$, and corresponds to the optimal branch where it is solid. (b) Maximized reset rate Γ_{max}/κ *vs.* $\tilde{g}/\kappa$ (we follow the red line from (a)). In (a) and (b), the parameter configurations A, B and C at which the reset dynamic was probed (see main text and Fig. 4) are indicated with colored symbols and the exceptional point is represented by a black cross.

Eq. (1), we derive the time-dependence of the population

$$P^{H}_{s|s_0}(t) = \left| \sum_k \langle s|\, \hat{A}_k\, |s_0\rangle\, e^{-i\lambda_k t} \right|^2 \qquad (2)$$

of state $|s\rangle \in \{|e,0\rangle, |f,0\rangle, |g,1\rangle\}$ during the reset. Here, $|s_0\rangle$ is the initial state of the system, λ_k are the eigenvalues of Hamiltonian (1) and $\hat{A}_k$ are operators that depend only on Hamiltonian (1) [34]. These populations oscillate at rates $2\text{Re}(\lambda_k)$ and decay exponentially at rates $2|\text{Im}(\lambda_k)|$. As the smallest decay rate dominates at long reset times, we define the reset rate as $\Gamma \equiv \min[2|\text{Im}(\lambda_k)|]$. The reset can be operated in two regimes [34]. In the low drive-power region hatched in Fig. 3a, the eigenvalues λ_k are purely imaginary: the reset is in an over-damped regime where the qutrit excited populations decay with no oscillation. When crossing the critical damping boundary, two eigenvalues abruptly display a finite real part and the reset enters an underdamped, oscillatory regime. The reset rate Γ is bounded by its maximum value $\kappa/3$ which it reaches on a line in parameter space, defining an optimal branch (solid red line in Fig. 3). The optimal branch intersects the critical-damping boundary at an exceptional point (black cross in Fig. 3) where all three eigenvalues are identical [42]. At this point, the reset has maximum rate and displays no oscillations. For a given $\tilde{g}$, there is a unique value of Ω_{ef} maximizing the reset rate to $\Gamma_{max}(\tilde{g})$. The parameter configuration then lies on the critical-damping boundary if $\tilde{g}$ is below its value at the exceptional point $\tilde{g}_{ep} = \sqrt{2/27}\kappa$ (red dashed line in Fig. 3), and on the optimal branch otherwise. As $\tilde{g}$ goes below $\tilde{g}_{ep}$, $\Gamma_{max}(\tilde{g})$ abruptly drops (Fig. 3b). Therefore, the ability to drive the f0-g1 transition with $\tilde{g} > \tilde{g}_{ep}$ is crucial to achieve fast reset.

We probed the reset dynamics at the three parame-

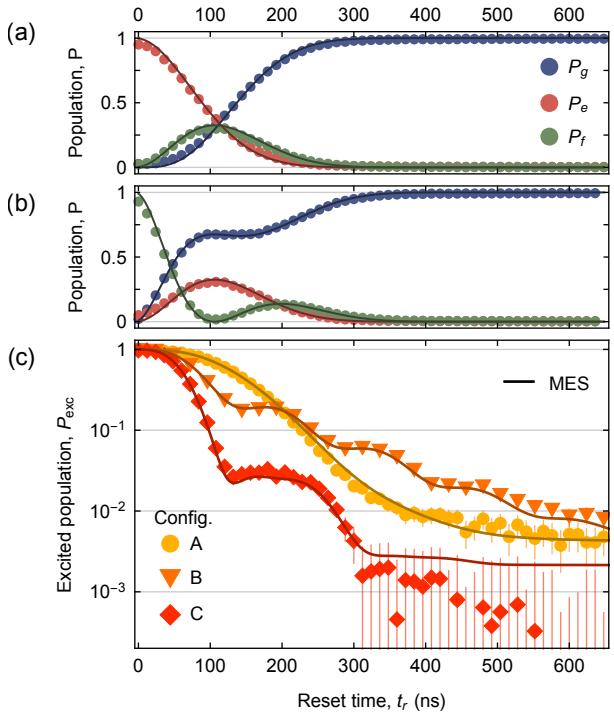

FIG. 4. Qutrit populations $P_{g,e,f}$ *vs.* reset time t_r with reset parameters in configuration A (see main text), and (a) system initialized in $|e,0\rangle$ or (b) in $|f,0\rangle$. The solid lines in (a) and (b) are calculated from Eq. (2). (c) Excited population P_{exc} as a function of reset time t_r, when the qutrit is initialized in $|e,0\rangle$, shown for reset parameter configurations A, B and C. The solid lines are calculated from a master equation simulation.

ter configurations labelled A, B and C in Fig. 3a. We initialize the transmon in $|e,0\rangle$ or $|f,0\rangle$, apply the reset drive pulses for a time t_r, and then readout the transmon with single-shot measurements, as illustrated in Fig. 1c. Utilizing the single-shot statistics, we correct for the qutrit state assignment errors, to determine the population of the qutrit with systematic errors below 0.3% [34]. We first probed the reset in configuration A ($\Omega_{ef}/2\pi = 1.5\,$MHz, $\tilde{g}/2\pi = 2.9\,$MHz), which is on the optimal branch and is the closest to the exceptional point. During the reset, the transmon state oscillates between $|g\rangle$, $|e\rangle$ and $|f\rangle$ while rapidly decaying to $|g\rangle$ on a time scale of 300 ns, independent of the initial state (Fig. 4a and b). The excited population $P_{exc} = P_e + P_f$ drops to below 1% without displaying any oscillations (Fig. 4c). The reset dynamics calculated from Eq. (2) is in excellent agreement with the data, as shown by the solid lines in Fig. 4a and b. When increasing the e-f drive to $\Omega_{ef}/2\pi = 3\,$MHz (B), the decaying state $|g,1\rangle$ is populated earlier. As a result, we observe that P_{exc} drops faster initially but at a slower rate at longer times since configuration B is not on the optimal branch (Fig. 4c). Because this parameter set realizes the under-damped regime, P_{exc} displays oscillatory features. Configuration C ($\Omega_{ef}/2\pi = 3\,$MHz, $\tilde{g}/2\pi = 4.8\,$MHz) is on the optimal branch and has higher drive rates than configuration A. Therefore, P_{exc} drops faster initially, and with the same long-time rate, leading to a more efficient reset. In this configuration, P_{exc} drops below 1% in only 280 ns, and below measurement errors ($\sim 0.3\%$) in steady-state (Fig. 4c), outperforming all existing measurement-based and microwave-driven reset schemes by an order of magnitude [34].

At long reset times, P_{exc} saturates to a non-zero steady-state value P_{exc}^{sat} because of transmon rethermalization. To fully capture the role of decoherence and rethermalization during the reset, we perform master equation simulations using only parameters extracted from independent measurements [34]. The numerical simulations are in excellent agreement with the data for all probed reset parameter configurations (solid lines in Fig. 4c) and yield $P_{exc}^{sat} = 0.2\%$ for configuration C, suggesting that the P_{exc}^{sat} achievable in our experiment is limited by transmon rethermalization. In this case, the excited population saturates at $P_{exc}^{sat} = k_\uparrow \tau$, where $k_\uparrow \simeq n_{th}/T_1$ is the rethermalization rate, with n_{th} the excited population at thermal equilibrium, and $\tau = \int_0^\infty [P_{e|e}^H + P_{f|e}^H](t)dt$ [34]. Therefore, faster drops of P_{exc}, obtained by increasing the drive rates along the optimal branch, result in lower steady-state excited populations (Fig. 4c). Other limitations, such as residual driving of the g-e transition by the e-f drive, and finite temperature of the resonator, are negligible for the presented parameters [34].

High transmon anharmonicity α combined with large transmon-resonator coupling g allows for reaching larger Ω_{ef} and $\tilde{g}$ without driving unwanted transitions [40]. Driving the reset at higher Rabi rates, we can reach the optimal branch, where $\Gamma = \kappa/3$, for larger values of κ. As a result, increasing g, α and κ maximizes Γ and optimizes the reset. Increasing these parameters also optimizes speed and fidelity of qubit readout without degrading the coherence and thermalization of the qubit, if Purcell filters are used [32, 34]. Therefore, our reset protocol performs best with a resonator designed for optimal readout. As an illustration, using the results of the present work, we calculate that implementing this reset protocol with the readout resonator of Ref. [32] would reset the qutrit below $P_{exc} = 0.1\%$ in 83 ns, and to a steady-state value $P_{exc}^{sat} = 1.6 \times 10^{-4}$ in 200 ns, provided that the f0-g1 Rabi rate exceeds $\sqrt{2/27}\kappa \simeq 2\pi \times 10\,$MHz.

In conclusion, we have demonstrated an unconditional all-microwave protocol to reset the state of a three-level transmon below 1% excitation in less than 280 ns. This reset scheme does neither require feedback, nor qubit tunability, not does it constrain device parameters or populate the readout resonator with a large number of photons. Furthermore, the protocol can conveniently be integrated in an architecture where the qubits are coupled to high bandwidth, Purcell-filtered resonators, in

order to perform rapid and high-fidelity quantum manipulations [43] and readout [32, 44]. However, in a multi-qubit system, the protocol's need for high f0-g1 drive power increases the sensitivity to cross-talk and can cause spurious driving of two-qubit transitions. Addressing these concerns in scaled up circuits will require improved shielding of drive lines, and careful selection of resonator and qubit frequencies. We did not observe any degradation of qubit coherence and operation fidelity in the presence of the reset drive tones [43], but a systematic study of these effects constitutes valuable future work.

We thank Christian Kraglund Andersen for helpful discussions. This work is supported by the European Research Council (ERC) through the "Superconducting Quantum Networks" (SuperQuNet) project, by National Centre of Competence in Research "Quantum Science and Technology" (NCCR QSIT), a research instrument of the Swiss National Science Foundation (SNSF), by the Office of the Director of National Intelligence (ODNI), Intelligence Advanced Research Projects Activity (IARPA), via the U.S. Army Research Office grant W911NF-16-1-0071, NSERC, the Canada First Research Excellence Fund and the Vanier Canada Graduate Scholarships and by ETH Zurich. The views and conclusions contained herein are those of the authors and should not be interpreted as necessarily representing the official policies or endorsements, either expressed or implied, of the ODNI, IARPA, or the U.S. Government. The U.S. Government is authorized to reproduce and distribute reprints for Governmental purposes notwithstanding any copyright annotation thereon.

[1] D. P. DiVincenzo, Fortschritte der Physik **48**, 771 (2000).
[2] P. Schindler, J. T. Barreiro, T. Monz, V. Nebendahl, D. Nigg, M. Chwalla, M. Hennrich, and R. Blatt, Science **332**, 1059 (2011).
[3] M. D. Reed, L. DiCarlo, S. E. Nigg, L. Sun, L. Frunzio, S. M. Girvin, and R. J. Schoelkopf, Nature **482**, 382 (2012).
[4] J. Chiaverini, D. Leibfried, T. Schaetz, M. Barrett, R. Blakestad, J. Britton, W. Itano, J. Jost, E. Knill, C. Langer, R. Ozeri, and D. Wineland, Nature **432**, 602 (2004).
[5] C. Monroe, D. M. Meekhof, B. E. King, S. R. Jefferts, W. M. Itano, D. J. Wineland, and P. Gould, Phys. Rev. Lett. **75**, 4011 (1995).
[6] F. Jelezko, T. Gaebel, I. Popa, A. Gruber, and J. Wrachtrup, Phys. Rev. Lett. **92**, 076401 (2004).
[7] J. M. Elzerman, R. Hanson, L. H. W. van Beveren, L. M. K. Vandersypen, and L. P. Kouwenhoven, Nature **430**, 431 (2004).
[8] M. V. G. Dutt, L. Childress, L. Jiang, E. Togan, J. Maze, F. Jelezko, A. S. Zibrov, P. R. Hemmer, and M. D. Lukin, Science **316**, 1312 (2007).
[9] L. J. Rogers, K. D. Jahnke, M. H. Metsch, A. Sipahigil, J. M. Binder, T. Teraji, H. Sumiya, J. Isoya, M. D. Lukin, P. Hemmer, and F. Jelezko, Phys. Rev. Lett. **113**, 263602 (2014).
[10] S. O. Valenzuela, W. D. Oliver, D. M. Berns, K. K. Berggren, L. S. Levitov, and T. P. Orlando, Science **314**, 1589 (2006), http://www.sciencemag.org/content/314/5805/1589.full.pdf.
[11] M. D. Reed, B. R. Johnson, A. A. Houck, L. DiCarlo, J. M. Chow, D. I. Schuster, L. Frunzio, and R. J. Schoelkopf, Appl. Phys. Lett. **96**, 203110 (2010).
[12] M. Mariantoni, H. Wang, T. Yamamoto, M. Neeley, R. C. Bialczak, Y. Chen, M. Lenander, E. Lucero, A. D. O'Connell, D. Sank, M. Weides, J. Wenner, Y. Yin, J. Zhao, A. N. Korotkov, A. N. Cleland, and J. M. Martinis, Science **334**, 61 (2011).
[13] J. E. Johnson, C. Macklin, D. H. Slichter, R. Vijay, E. B. Weingarten, J. Clarke, and I. Siddiqi, Phys. Rev. Lett. **109**, 050506 (2012).
[14] D. Ristè, J. G. van Leeuwen, H.-S. Ku, K. W. Lehnert, and L. DiCarlo, Phys. Rev. Lett. **109**, 050507 (2012).
[15] D. Ristè, C. C. Bultink, K. W. Lehnert, and L. DiCarlo, Phys. Rev. Lett. **109**, 240502 (2012).
[16] P. Campagne-Ibarcq, E. Flurin, N. Roch, D. Darson, P. Morfin, M. Mirrahimi, M. H. Devoret, F. Mallet, and B. Huard, Phys. Rev. X **3**, 021008 (2013).
[17] Y. Salathé, P. Kurpiers, T. Karg, C. Lang, C. K. Andersen, A. Akin, S. Krinner, C. Eichler, and A. Wallraff, Phys. Rev. Applied **9**, 034011 (2018).
[18] K. Geerlings, Z. Leghtas, I. M. Pop, S. Shankar, L. Frunzio, R. J. Schoelkopf, M. Mirrahimi, and M. H. Devoret, Phys. Rev. Lett. **110**, 120501 (2013).
[19] D. J. Egger, M. Ganzhorn, G. Salis, A. Fuhrer, P. Mueller, and S. Filipp, ArXiv:1802.08980 (2018), arXiv:1802.08980 [quant-ph].
[20] M. Boissonneault, J. M. Gambetta, and A. Blais, Phys. Rev. A **79**, 013819 (2009).
[21] D. H. Slichter, R. Vijay, S. J. Weber, S. Boutin, M. Boissonneault, J. M. Gambetta, A. Blais, and I. Siddiqi, Phys. Rev. Lett. **109**, 153601 (2012).
[22] D. Sank, Z. Chen, M. Khezri, J. Kelly, R. Barends, B. Campbell, Y. Chen, B. Chiaro, A. Dunsworth, A. Fowler, and et al., Physical Review Letters **117**, 190503 (2016).
[23] A. G. Fowler, Phys. Rev. A **88**, 042308 (2013).
[24] M. Grajcar, S. H. W. van der Ploeg, A. Izmalkov, E. Il'ichev, H.-G. Meyer, A. Fedorov, A. Shnirman, and G. Schön, Nat. Phys. **4**, 612 (2008).
[25] D. Basilewitsch, R. Schmidt, D. Sugny, S. Maniscalco, and C. P. Koch, arXiv:1703.04483 (2017).
[26] K. W. Murch, U. Vool, D. Zhou, S. J. Weber, S. M. Girvin, and I. Siddiqi, Phys. Rev. Lett. **109**, 183602 (2012).
[27] S. P. Premaratne, F. C. Wellstood, and B. S. Palmer, Phys. Rev. A **96**, 043858 (2017).
[28] K. Y. Tan, M. Partanen, R. E. Lake, J. Govenius, S. Masuda, and M. Mttnen, Nature Communications **8**, 15189 (2017).
[29] Y. Liu, S. Shankar, N. Ofek, M. Hatridge, A. Narla, K. M. Sliwa, L. Frunzio, R. J. Schoelkopf, and M. H. Devoret, Phys. Rev. X **6**, 011022 (2016).
[30] J. Kelly, R. Barends, B. Campbell, Y. Chen, Z. Chen, B. Chiaro, A. Dunsworth, A. G. Fowler, I.-C. Hoi, E. Jeffrey, A. Megrant, J. Mutus, C. Neill, P. J. J. O'Malley, C. Quintana, P. Roushan, D. Sank, A. Vainsencher, J. Wenner, T. C. White, A. N. Cleland, and J. M. Mar-

tinis, Phys. Rev. Lett. **112**, 240504 (2014).
[31] J. Gambetta, W. A. Braff, A. Wallraff, S. M. Girvin, and R. J. Schoelkopf, Phys. Rev. A **76**, 012325 (2007).
[32] T. Walter, P. Kurpiers, S. Gasparinetti, P. Magnard, A. Potocnik, Y. Salathé, M. Pechal, M. Mondal, M. Oppliger, C. Eichler, and A. Wallraff, Phys. Rev. Applied **7**, 054020 (2017).
[33] M. Pechal, L. Huthmacher, C. Eichler, S. Zeytinoğlu, A. A. Abdumalikov Jr., S. Berger, A. Wallraff, and S. Filipp, Phys. Rev. X **4**, 041010 (2014).
[34] "See Supplemental Material at [url] for an overview and comparison to prior art, for details about the sample fabrication and parameters, for details about the fit functions for the calibration procedure, for a derivation of the reset operating regimes, for a description of the readout method, for a discussion of the limitations of the reset, and for a description of the master equation simulations.".
[35] J. Koch, T. M. Yu, J. Gambetta, A. A. Houck, D. I. Schuster, J. Majer, A. Blais, M. H. Devoret, S. M. Girvin, and R. J. Schoelkopf, Phys. Rev. A **76**, 042319 (2007).
[36] J. A. Schreier, A. A. Houck, J. Koch, D. I. Schuster, B. R. Johnson, J. M. Chow, J. M. Gambetta, J. Majer, L. Frunzio, M. H. Devoret, S. M. Girvin, and R. J. Schoelkopf, Phys. Rev. B **77**, 180502 (2008).
[37] R. Bianchetti, S. Filipp, M. Baur, J. M. Fink, C. Lang, L. Steffen, M. Boissonneault, A. Blais, and A. Wallraff, Phys. Rev. Lett. **105**, 223601 (2010).
[38] B. Yurke, M. L. Roukes, R. Movshovich, and A. N. Pargellis, Appl. Phys. Lett. **69**, 3078 (1996).
[39] C. Eichler and A. Wallraff, EPJ Quantum Technology **1**, 2 (2014).
[40] S. Zeytinoğlu, M. Pechal, S. Berger, A. A. Abdumalikov Jr., A. Wallraff, and S. Filipp, Phys. Rev. A **91**, 043846 (2015).
[41] S. Gasparinetti, S. Berger, A. A. Abdumalikov, M. Pechal, S. Filipp, and A. J. Wallraff, Science Advances **2**, e1501732 (2016).
[42] W. D. Heiss, Journal of Physics A: Mathematical and General **37**, 2455 (2004).
[43] P. Kurpiers, P. Magnard, T. Walter, B. Royer, M. Pechal, J. Heinsoo, Y. Salathé, A. Akin, S. Storz, J.-C. Besse, S. Gasparinetti, A. Blais, and A. Wallraff, Nature **558**, 264 (2018).
[44] J. Heinsoo, C. K. Andersen, S. K. A. Remm, T. Walter, Y. Salathé, S. Gasparinetti, J.-C. Besse, A. Potočnik, C. Eichler, and A. Wallraff, ArXiv e-prints (2018).